


# Small Intestinal Endocrine Cell Derived Exosomal ACE2 Protects Islet $\beta$ -Cell Function by Inhibiting the Activation of NLRP3 Inflammasome and Reducing $\beta$ -Cell Pyroptosis

Songtao Yang , Jie Cao, Ying Wang, Qi Chen, Fangyu Li, Yuanyuan Gao, Rui Li, Li Yuan

Department of Endocrinology, Union Hospital, Tongji Medical College, Huazhong University of Science and Technology, Wuhan, 430022, People's Republic of China

Correspondence: Li Yuan, Department of Endocrinology, Union Hospital, Tongji Medical College, Huazhong University of Science and Technology, Wuhan, 430022, People's Republic of China, Email [yuanli18cn@126.com](mailto:yuanli18cn@126.com)

**Background:** The “gut-islets axis” is an important endocrine signaling axis that regulates islets function by modulating the gut microbiota and endocrine metabolism within the gut. However, the specific mechanisms and roles of the intestine in islets regulation remain unclear. Recent studies investigated that exosomes derived from gut microbiota can transport signals to remotely regulate islets  $\beta$ -cell function, suggesting the possibility of novel signaling pathways mediated by gut exosomes in the regulation of the “gut-islet axis.”

**Methods:** The exosomes were isolated from the intestinal enteroendocrine cell-line STC-1 cells culture supernatants treated with palmitate acid (PA) or BSA. Metabolic stress models were established by separately subjecting MIN6 cells to PA stimulation and feeding mice with a high-fat diet. Intervention with exosomes in vitro and in vivo to assess the biological effects of exosomes on islets  $\beta$  cells under metabolic stress. The Mas receptor antagonist A779 and ACE2ko mice were used to evaluate the role of exosomal ACE2.

**Results:** We found ACE2, a molecule that plays a crucial role in the regulation of islets function, is abundantly expressed in exosomes derived from STC-1 under physiological normal condition (NCEO). These exosomes cannot only be taken up by  $\beta$ -cells in vitro but also selectively transported to the islets in vivo. Following intervention with NCEO, both Min6 cells in a lipotoxic environment and mice on a high-fat diet exhibited significant improvements in islets  $\beta$ -cell function and  $\beta$ -cell mass. Further investigations demonstrated that these protective effects are attributed to exosomal ACE2, as ACE2 inhibits NLRP3 inflammasome activation and reduces  $\beta$ -cell pyroptosis.

**Conclusion:** ACE2-enriched exosomes from the gut can selectively target islets, subsequently inhibiting NLRP3 inflammasome activation and  $\beta$  cell pyroptosis, thereby restoring islets  $\beta$  cell function under metabolic stress. This study provides novel insights into therapeutic strategies for the prevention and treatment of obesity and diabetes.

**Keywords:** exosomes, ACE2, islets  $\beta$  cell, the NLRP3 inflammasome

## Introduction

The incidence of metabolic syndrome and diabetes has been steadily increasing over the years, with a notable trend of affecting younger individuals.<sup>1</sup> As diabetes progresses and poor disease management, the rates of disability and mortality caused by diabetes and its complications are expected to rise significantly. Preserving the function of islets  $\beta$  cells has emerged as a pivotal topic in the field of prevention and treatment of metabolic syndrome and diabetes. The discovery of intestinal hormones such as GLP-1 (glucagon-like peptide 1) and GIP (glucose-dependent insulinotropic peptide) have laid the initial groundwork for establishing a cross-talk between the intestine and the islets. Building upon the “gut-islets axis” regulatory theory, the development and application of GLP-1 receptor agonists in the domain of diabetes treatment have ushered in a new paradigm for glycemic control in diabetes therapy. Consequently, the “gut-islets axis” regulatory theory has rapidly become a focal point of research attention.

The “gut-islets axis” is an important endocrine signaling axis that involves the regulation and communication of islets function by the gut microbiota and intestinal endocrine metabolism.<sup>2</sup> Recent research has revealed that the intestine serves not only as the site for nutrient digestion and absorption but also as the largest endocrine organ in the body. It maintains the regulation of local intestinal microenvironment, distant tissues, and whole-body metabolism through an extensive endocrine system composed of enteroendocrine cells and intestinal microbiota.<sup>3,4</sup>

Emerging studies have shown that, in addition to gut-derived endocrine hormones, intestinal cells can also exert regulatory control over distant tissues by secreting extracellular vesicles known as exosomes. These exosomes, ranging from 40 to 160 nm in size and containing functional proteins, mRNA, and miRNA, play specific biological effects under different pathological and physiological conditions.<sup>5</sup> Due to their diverse characteristics, these extracellular vesicles have become an indispensable component of intestinal endocrine regulation. The discovery of intestinal-originated exosomes containing various bioactive substances has further enriched and expanded the theoretical implications of the “gut-islets axis”,<sup>6,7</sup> revealing novel regulatory mechanisms that were previously unknown.

The classical understanding of ACE2 primarily involves its role as a crucial component of the renin–angiotensin system (RAS) counteracting the ACE-signaling pathway in the ACE2/Ang1-7/Mas axis.<sup>8</sup> Due to its capacity to reduce the levels of angiotensin II (Ang II) and antagonize its effects, ACE2 has garnered considerable attention for its dual action akin to RAS inhibitors ACEI and ARB. In our earlier investigations, we found that ACE2, on the one hand, interacts with the Mas receptor to inhibit oxidative stress and inflammatory response, positively regulating the function and differentiation status of islets  $\beta$  cells, thereby improving islets microcirculation and protecting the endothelial cell function within the islets.<sup>9,10</sup> On the other hand, ACE2 serves as a membrane-bound ligand involved in amino acid transport, participating in the regulation of islets function through the modulation of amino acid transport and absorption in the upstream region of the intestine.<sup>11</sup> Previous studies have indicated that ACE2 is closely associated with the integrity of the intestinal barrier function,<sup>12</sup> with ACE2-deficient mice being more susceptible to intestinal barrier damage and inflammations.<sup>13</sup> Furthermore, the regulation of neutral amino acid transporter protein B0AT1 expression by ACE2 further demonstrates the critical role of ACE2 in regulating amino acid absorption, gut microbiota ecology, and intestinal inflammation.<sup>14,15</sup> Therefore, when changes occur in the microenvironment, the intestine may secrete more ACE2 to maintain intestinal homeostasis. Here, we further investigated these ACE2 enriched exosomes secreted by small intestinal endocrine cells can not only be directly taken up by islets  $\beta$  cells in vitro but also demonstrate the ability to undergo long-distance targeted transport to the islets in vivo, potentially serving as a plausible source of ACE2 within the islets. These findings suggest that ACE2 may regulate islets function through a dual mechanism involving both local modulation within the islets and long-distance transport via the “gut-islets axis”. However, the regulation of islets  $\beta$ -cell function by intestinal exosomal ACE2 within the “gut-islets axis” and its molecular mechanisms, is currently unclear.

An increasing number of research indicates that chronic, low-grade systemic inflammation often accompanies obesity, insulin resistance, and type 2 diabetes mellitus (T2DM), promoting the progression from obesity to T2DM.<sup>16</sup> During the progression from obesity to T2DM, the expression of IL-1 $\beta$  increases in circulation and within the pancreatic islets. IL-1 $\beta$  is considered one of a crucial driving factors in the disease, as elevated pro-inflammatory cytokines can lead to insulin resistance and impaired glucose tolerance by antagonizing insulin signaling. Simultaneously, local inflammation infiltrates the islets, combined with the toxic effects of glucose, resulting in accelerated cell death and a significant loss of  $\beta$ -cell mass, severely impairing the insulin-secreting capacity of the remaining  $\beta$ -cells. The maturation and secretion of IL-1 $\beta$  are primarily regulated through inflammasomes, especially the NLRP3 inflammasome, which is also considered a sensor for metabolic danger. The NLRP3 inflammasome is consisting of a sensor (nucleotide-binding oligomerization domain (NOD)-like receptor and pyrin domain-containing 3 (PYD); NLRP3), an adapter (apoptosis-associated speck-like protein, containing a CARD; ASC), and an effector (Pro-caspase 1).<sup>17</sup> Once the sensor detects pathogens, homeostatic imbalance, or endogenous danger signals, the NLRP3 inflammasome spontaneously activates Pro-caspase 1, transforming it into an active form of Caspase 1. Activated Caspase 1 then cleaves and activates more than 70 substrate proteins, including the pro-inflammatory cytokines IL-1 $\beta$  and IL-18.<sup>18</sup> Moreover, the cleavage of GSDMD (Gasdermin D) by Caspase 1 produces the N-terminal fragment of GSDMD (N-GSDMD). N-GSDMD penetrates the cell membrane, forming a non-selective pore with an inner diameter of approximately 10–14 nm,<sup>19</sup> leading to cellular swelling and ultimately resulting in pyroptosis.<sup>20,21</sup> The fragmented and disintegrated cells will also release their intracellular

inflammasomes and inflammatory factors, further exacerbating the inflammatory environment.<sup>22</sup> The assembly of the NLRP3 inflammasome into a trimer, required for activation in response to endogenous danger signals, has been demonstrated in various studies. It is noteworthy that the activation of NF $\kappa$ B has been confirmed to initiate the assembly of the NLRP3 inflammasome,<sup>23–27</sup> and with the fact that the important relationship between ACE2, NF $\kappa$ B and the NLRP3 inflammasome is gradually revealed.<sup>28–31</sup> This also opens up new directions for exploring the regulatory initiation points, specific molecular pathways, and mechanisms behind the “gut-islets axis”.

Our study focuses on the regulatory role of intestinal-originated exosomal ACE2 in islets function, aiming to reshape the islet microenvironment and explore novel therapeutic strategies to protect islets  $\beta$  cell function. These findings open up new avenues for future treatments of obesity and diabetes, providing promising prospects for application and paving the way for further research in this field.

## Methods

### Exosome Isolation, Identification and Labeling

Cell culture supernatants were collected from the intestinal enteroendocrine cell line STC-1 cells within passage 10 treated with PA or BSA, when the cells became 80–90% confluent. STC-1 cells were cultured in RPMI-1640 (Gibco, USA) with 10% exosome-free fetal bovine serum (HYCEZMBIO, Wuhan, China) and 1% sodium pyruvate solution (BasalMedia, Shanghai, China). Exosomes were isolated as previous.<sup>32</sup> The supernatants were centrifuged at 1000g for 10 min and centrifuged at 3000g for 30 min at first; thereafter, the supernatants were centrifuged at 9000g for 40min, and the supernatants were then ultracentrifuged (Beckman Coulter, Shanghai, Chian) 120000g for 70 min to obtain exosomes. Exosome was washed with PBS and ultracentrifuged under the same conditions, after which the exosomes were resuspended with PBS and filtered using 0.2  $\mu$ m filters (Millipore, USA). NCEXO: exosomes isolated from STC-1 cells culture supernatants under normal condition; PAEXO: exosomes isolated from PA stimulated STC-1 cells culture supernatants.

The purified exosomes were stained with 2% uranyl acetate and added to a copper grid at 4 °C. Thereafter, transmission electron microscopy (TEM) (TECNAI G2 spirit FEI, Netherlands) was performed to assess exosome morphology, and NTA (Particle Metrix ZetaView PMX 110) was used for particle size analysis. The exosome markers were determined by Western blot. Briefly, an equal amount of 50  $\mu$ g total protein was separated by SDS-PAGE (ACE Biotechnology, China), transferred onto the PVDF membrane (Millipore, USA), and then incubated overnight with primary antibodies specific for ALIX, CD9, and TSG101. Thereafter, they were incubated with HRP-conjugated antibody (Servicebio, Wuhan, China) for 1h. An ECL substrate kit (P10060, NCM Biotech, China) and the BioSpectrum 600 Imaging System (UVP, CA, USA) were used for exposure.

The green dye PKH67 (Sigma MINI67-1KT, USA) was used for exosome tracing following the manufacturer's instructions. The uptake of labeled exosomes was then assessed through the combination with Min6 cells; immunofluorescence was used for measuring. The exosome tracing in vivo was evaluated using the in vivo imaging system (Bruker MI SE 7.2 software, Bruker, German). The images were analyzed using Bruker MI SE 7.2 software.

### Cell Culture and Treatment

The mouse insulinoma cell line MIN6 was purchased from the ATCC and cultured in RPMI-1640 (Gibco) with 15% fetal bovine serum and 50  $\mu$ mol/L of beta-mercaptoethanol at 37°C in an atmosphere of 95% humidified air and 5% CO<sub>2</sub>. The stimulations were added when MIN6 cells reached 80% confluency. MIN6 cells were cultured in a corresponding medium containing 0.5 mmol/L of palmitic acid (PA) (Solarbio, Beijing, China) for 48 hours with or without NCEXO/PAEXO or A1-7/A779 (TargetMol, Shanghai, China). The intestinal enteroendocrine cell line STC-1 was purchased from Wuhan Warner Biotechnology company, Wuhan, China and cultured in RPMI-1640 (Gibco, USA) with 10% fetal bovine serum and 1% sodium pyruvate solution. The exosome-free FBS was obtained from HYCEZMBIO, Wuhan, China.

Mouse primary islets isolation as was performed using previously described protocols.<sup>33</sup> Briefly, after anesthetizing the mice, collagenase dissolved in D-Hank's solution was injected into their pancreatic ducts, followed by digestion at 37 degrees Celsius for 10 minutes. After digestion, large tissue fragments were filtered out, and the pancreatic islet cells were transferred to complete culture medium. Finally, pancreatic islets were manually selected under a microscope and transferred to new culture medium.

## 5-Ethynyl-2'-Deoxyuridine(EdU) Assay

After the cell treatment, EdU was performed to assess the levels of cell proliferation using a commercial BeyoClick EdU-488 kit (C0071S, Beyotime, Wuhan, China) according to the manufacturer's instructions. The images were observed by a confocal microscope (Nikon, Tokyo, Japan).

## Cell Viability Analysis

MIN6 cells were seeded and grown in 96-well plates at  $1 \times 10^4$  cells/well (three replicate wells) overnight. Cell viability was assessed by a CCK-8 (Dojindo Laboratories, Kumamoto, Japan) assay according to the manufacturer's protocol after the cell treatment.

## Apoptosis Analysis

After specific cell treatment, the Min6 cell apoptosis rate was performed using an Annexin V and PI apoptosis kit (Proteintech, PF00005) according to the manufacturer's protocol and then measured by flow cytometry (Becton, Franklin Lake, NJ, USA). The results were analyzed using FlowJov.10.6.2 software (LLC, Ashland, USA)

## Glucose-Stimulated Insulin Secretion Assay(GSIS)

Insulin secretion in Min6 cells was carried out using previous protocol.<sup>11</sup> After 48h treatment of PA with or without NCEXO/PAEXO, the cells were incubated in HEPES-balanced Krebs-Ringer bicarbonate buffer (KRBH) with 2.8 mmol/l glucose for 30 min. Then, the supernatants were collected, and cells were washed and then incubated in KRBH containing 16.7 mmol/l glucose for 1h. The supernatants were collected again for later measurement.

## Animals

Mice groups: (1) SD group: male C57BL/6J wild-type mice fed a standard chow diet. (2) HFD group: male C57BL/6J WT mice fed a high-fat diet. (3) NCEXO group: male C57BL/6J WT mice fed a high-fat diet and treated with NCEXO. (4) PAEXO group: male C57BL/6J WT mice fed a high-fat diet and treated with PAEXO. (5) NCEXO+A779 group: male C57BL/6J WT mice fed a high-fat diet and treated with NCEXO and A779. (6) KOSD group: male ACE2<sup>ko</sup> mice fed a standard chow diet. (7) KOHFD group: male ACE2<sup>ko</sup> mice fed a high-fat diet. (8) KOHFD+NCEXO group: male ACE2<sup>ko</sup> mice fed a high-fat diet and treated with NCEXO. (9) AAV-NC HFD group: male C57BL/6J WT mice injected with AAV-NC fed a high-fat diet. (10) AAV-ACE2 HFD group: male C57BL/6J WT mice injected with AAV-ACE2 fed a high-fat diet. (n = 3–8 mice/group)

6-week-old male C57BL/6J mice were obtained from Beijing HFK Biotechnology Co., Ltd. 6-week-old ACE2<sup>ko</sup> mice on a C57BL/6J background were obtained from the Institute of Laboratory Animal Science, Chinese Academy of Medical Sciences. The standard-diet group and the ACE2<sup>ko</sup> group were fed a standard chow diet (SD, 20% protein, 70% carbohydrates, and 10% fat). The remaining mice were fed a high-fat diet (HFD; Research Diets, D12492, 20% protein, 20% carbohydrates, and 60% fat) for 3 months to induce insulin resistance. The mice with insulin resistance at week 12 were then treated with NCEXO/PAEXO, A779 or AAV-NC/AAV-ACE2. The mice were sacrificed at the week 16.

At week 10, AAV-NC mice and AAV-ACE2 mice were injected via tail vein with  $3 \times 10^{11}$  adeno-associated virus-negative control (AAV-NC) per mouse or  $3 \times 10^{11}$  adeno-associated virus-based ACE2 overexpression (AAV-ACE2) per mouse (serotype: AAV9), respectively. The other groups were given the equivalent volume of PBS by tail vein injection.

All mice were housed in a specific pathogen-free animal laboratory in a 12-hour light and 12-hour darkness cycle at room temperature. The body weight, food intake, and fasting blood glucose (FBG) of mice were measured every two weeks. The mice were sacrificed at the week 16. Animals applied in this study were followed the Guideline for ethical review of animal welfare of laboratory animals published by the China National Standardization Management Committee (publication No. GB/T 35892–2018). All of the experiments were approved by the Institutional Animal Care and Use Committee of Huazhong University of Science and Technology, Hubei Province, China (IACUC Number: 3417).

## Fasting Blood Glucose, Intraperitoneal Insulin Tolerance Tests and Intraperitoneal Glucose Tolerance Tests

The fasting blood glucose (FBG) levels in mice were assessed using a blood glucose meter (LifeScan, USA) following an overnight-fasting period. The intraperitoneal insulin tolerance tests (IPITT) were performed in mice by the injection of insulin (0.75 U/kg, i.p.) after mice were fasted overnight, and the intraperitoneal glucose tolerance tests (IPGTT) were performed by injecting glucose (2 g/kg, i.p.) after mice were fasted overnight; plasma glucose levels was measured at 0, 15, 30, 60, 90 minutes post-injection in IPITT and at 0, 30, 60, 90, 120 minutes post-injection in IPGTT.<sup>11</sup>

## Western Blotting

Protein from cells or pancreatic tissue was extracted in RIPA lysis buffer (NCE Biotech, China) with protease and phosphatase inhibitors. Protein samples were separated by SDS-PAGE and transferred to a PVDF membrane (Millipore, USA). The membrane was incubated with primary antibodies ([Supplementary Table 1](#)) overnight at 4 °C and were incubated in secondary antibodies (diluted 1:3000) for 1 hour at room temperature. Finally, the membranes were visualized with an ECL reagent (NCE Biotech, China) and measured. The Protein Marker was 180kDa Plus Prestained Protein Marker (MP201, Vazyme, China)

## qRT-PCR

Total RNA from MIN6 cells or pancreas tissue was extracted using TRIzol reagent (Takara Shuzo Co., Ltd., Kyoto, Japan), and the cDNA was synthesized using a Prime Script RT reagent kit (Takara Biotechnology Co. Ltd., Japan). Then qPCR was performed in a LightCycler480-PCR system (Roche Diagnostics, Mannheim). The relative transcript levels of the objective gene were normalized to  $\beta$ -actin and calculated by the  $2^{-\Delta\Delta CT}$  method. The primer sequences are listed in [Supplementary Table 2](#).

## Immunohistochemistry

Firstly, pancreatic paraffin sections were treated in an eco-friendly dewaxing solution for 40 minutes (G1128; Servicebio, Wuhan, China), followed by sequential hydration in 100%, 100%, 95%, 85%, and 70% ethanol and distilled water for 5 minutes each. Secondly, after dewaxing, the sections were placed in sodium citrate buffer, heated on high for 7 minutes, adjusted for evaporation, heated on medium for 7 minutes, adjusted again, and heated on medium for 5 minutes, followed by cooling. Thirdly, after reaching room temperature, the sections were washed three times in PBS for 10 minutes each on a shaker. After washing, tissue outlines were marked, and 50  $\mu$ L of 3% hydrogen peroxide was added to each section, followed by incubation at room temperature for 10 minutes. Fourthly, the sections were washed three times in PBS for approximately 10 minutes each on a shaker, then 50  $\mu$ L of 10% goat serum (G1208; Servicebio, Wuhan, China) was added to each section, and all sections were closed in a 37°C oven for 1 hour. Fifthly, after closure, the sections were washed three times in PBS for 10 minutes each on a shaker, followed by the addition of 50  $\mu$ L of antibodies against CD34 or CD31 overnight at 4°C (CD34: abcam ab81289; CD31: abcam ab182981). Sixthly, after primary antibody incubation, the sections were placed in a 37°C oven for 1 hour, then washed three times in PBS for 10 minutes each on a shaker. Subsequently, fluorescent secondary antibodies (GB1210; Servicebio, Wuhan, China) corresponding to the species source were added under dark conditions, followed by incubation in a 37°C oven for 1 hour. Seventhly, after secondary antibody incubation, the sections were washed three times in PBS for 10 minutes each on a shaker. DAB staining solution was added to the outlines, and staining was terminated by gently rinsing off the color under a microscope upon observation of brown-yellow color. Lastly, tissue sections were stained with hematoxylin for 2 minutes, washed with water, differentiated in 1% hydrochloric acid alcohol for a few seconds, treated with 1% ammonia water for 1 minute, washed again, and observed under a microscope. After staining, sections were sequentially treated with 70%, 85%, 95%, 100%, and 100% ethanol and xylene for several minutes each, and then sealed with neutral adhesive. Images were analyzed at identical exposure conditions using a light microscope.

## Immunofluorescence

The paraffin sections of pancreas were deparaffinized with xylene and then dehydrated in 100%, 95%, 85%, 70% ethanol for 5 min, respectively. The sections were incubated with primary antibodies overnight at 4°C (Primary antibodies were

listed in [Supplementary Table 1](#)). After PBS washing, the sections were incubated with secondary antibody (FITC, CY3, Servicebio) for 1h, and nuclei were stained with DAPI (Servicebio, Wuhan, China) at room in the dark. The images were analyzed by a confocal microscope (Nikon, Tokyo, Japan).

Image J software was used to determine the fluorescence density of captured images and conducted associated statistical analyses (calculation of  $\beta$ -cell mass and  $\alpha$ -cell mass: the mass of  $\beta$ -cells and  $\alpha$ -cells were determined by calculating the total area of pancreatic slices stained positively for insulin immunofluorescence ( $\beta$ -cells) or glucagon immunofluorescence ( $\alpha$ -cells), divided by the total area of pancreatic slices (%) and multiplied by the pancreatic weight (mg) obtained at the time of animal sacrifice).

## Enzyme-Linked Immunosorbent Assay (ELISA)

ELISA was used to assess the levels of circulating insulin and IL-1 $\beta$  in mice. The blood samples were collected in tubes containing EDTA from the tail vein of fasting mice during the IPGTT test. The insulin and IL1 $\beta$  levels were measured using a commercial ELISA kit (KE10089 and KE10003, Proteintech, China) following the manufacturer's instructions. The absorbance at 450 nm was detected using a microplate reader (PerkinElmer, Waltham, MA, USA).

## Statistical Analysis

The data were analyzed and processed by GraphPad Prism 9.5 software. Differences in numeric parameters between two groups were assessed with an unpaired two-tailed *t* test, and one-way or two-way ANOVA was used for comparison among multiple groups. All data were presented as the mean  $\pm$  standard deviation, and  $p < 0.05$  was considered statistically significant. The entirety of the experiments was repeated at least three times.

## Results

### Characteristics of Exosomes from Small Intestinal Endocrine Cells and Exosomes Tracing

Firstly, we assessed the exosomes secreted by small intestinal enteroendocrine cells STC-1 under various pathological and physiological conditions, namely NCEXO and PAEXO. Evaluation was conducted using transmission electron microscopy (TEM), nanoparticle tracking analysis (NTA), and Western blot (WB). TEM revealed that these extracellular vesicles exhibited cup-shaped or spherical morphology ([Figure 1A](#)), consistent with previous reports.<sup>5</sup> The results of WB confirmed the presence of exosomal surface markers such as CD9, ALIX, and TSG101 in these particles ([Figure 1B](#)). NTA analysis further demonstrated that the size of these particles ranged between 30 to 200nm, aligning with the reported size range of exosomes<sup>5</sup> ([Figure 1C](#)). These findings collectively confirm that the isolated extracellular vesicles are exosomes. Thereafter, we labeled NCEXO and PAEXO with PKH67 and performed in vitro and in vivo tracking experiments. We observed that both NCEXO and PAEXO were taken up by Min6 cells after 24 hours of co-culture ([Figure 1D](#)). Furthermore, in vivo tracking indicated that NCEXO and PAEXO exhibited targeting capability towards the pancreatic islets, providing valuable insights for the frequency of exosome injections in future in vivo experiments as well ([Figure 1E and F](#)).

### The NCEXO Contains Abundant ACE2 and Can Promote Proliferation and Reduce Apoptosis of Islets $\beta$ -Cells in vitro

In pursuit of a deeper understanding of the disparities between NCEXO and PAEXO, a series of analyses was conducted, revealing that in contrast to PAEXO, NCEXO exhibited a substantial abundance of ACE2, which is a key regulator of islet functionality ([Figure 2A and B](#)). To investigate the effects of NCEXO and PAEXO on islets  $\beta$ -cells, an initial assessment of optimal exosome intervention concentrations was conducted using Min6 cell. Under conditions of lipid-induced toxicity, varying concentrations of exosome interventions were administered. The findings revealed that at a concentration of 100  $\mu$ g/mL of exosomes, cellular viability could be restored to a comparatively desirable level ([Figure 2C](#)). Flow cytometry analysis was performed to assess the apoptotic status of Min6 cells following a 48h PA intervention. The results revealed that prolonged exposure to a lipid-toxic environment substantially elevated the

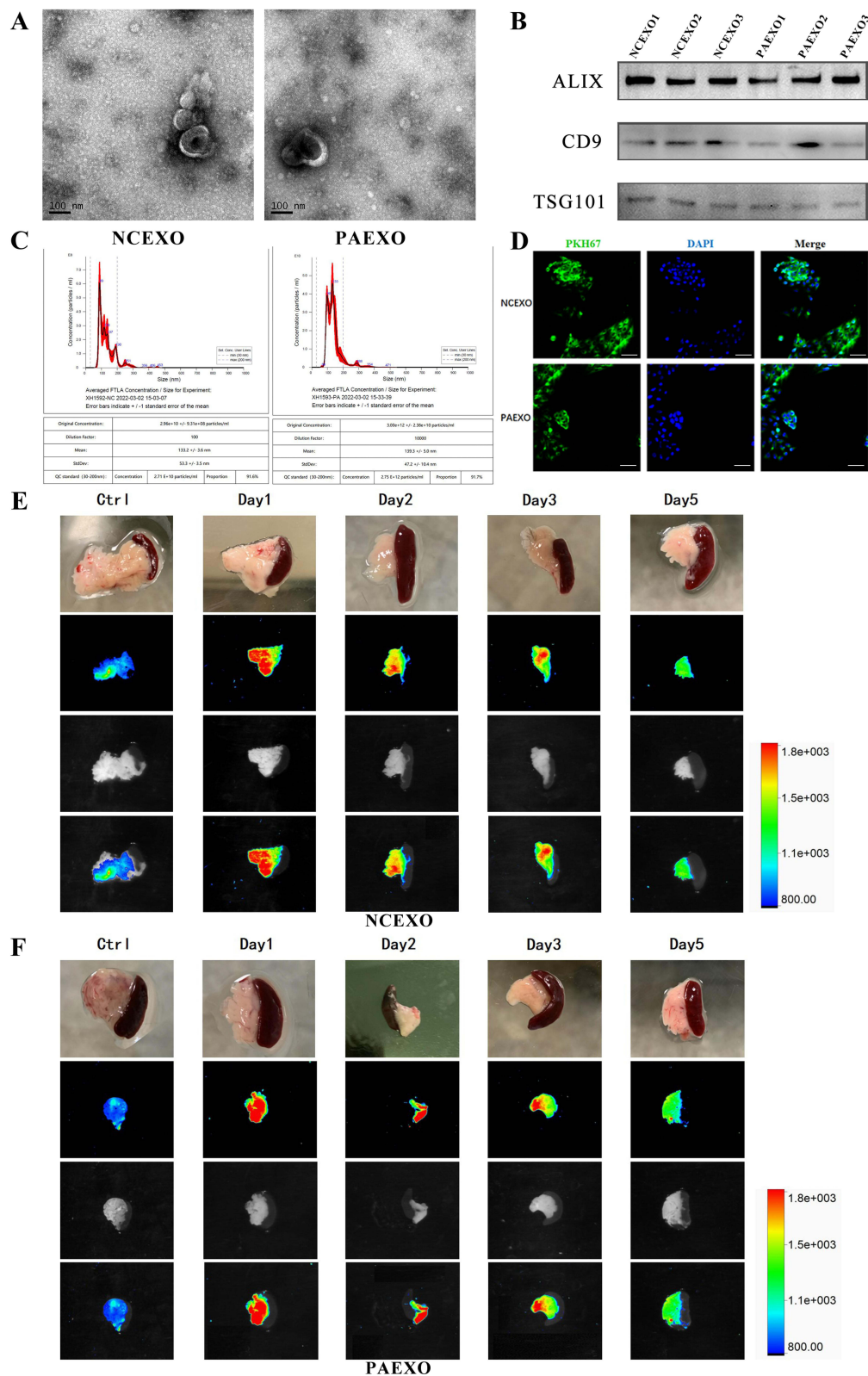


**Figure 1** Exosome isolation, identification and tracing. **(A)** Representative images of the isolated exosomes observed by TEM. Bar = 100 $\mu$ m. **(B)** WB showed the biomarkers level of CD 9, ALIX and TSG 101 in the isolated exosomes. **(C)** The size and amount of extracellular particles measured by NTA. **(D)** PKH67-labeled exosomes were absorbed by Min6 observed by a confocal microscope (Nikon, Tokyo, Japan). Bar = 50 $\mu$ m. The NCEXO **(E)** and PAEXO **(F)** tracing in vivo was evaluated by the in vivo imaging system (Bruker MI SE 7.2 software, Bruker, German). The fluorescence images were taken at day 1, 2, 3, 5.

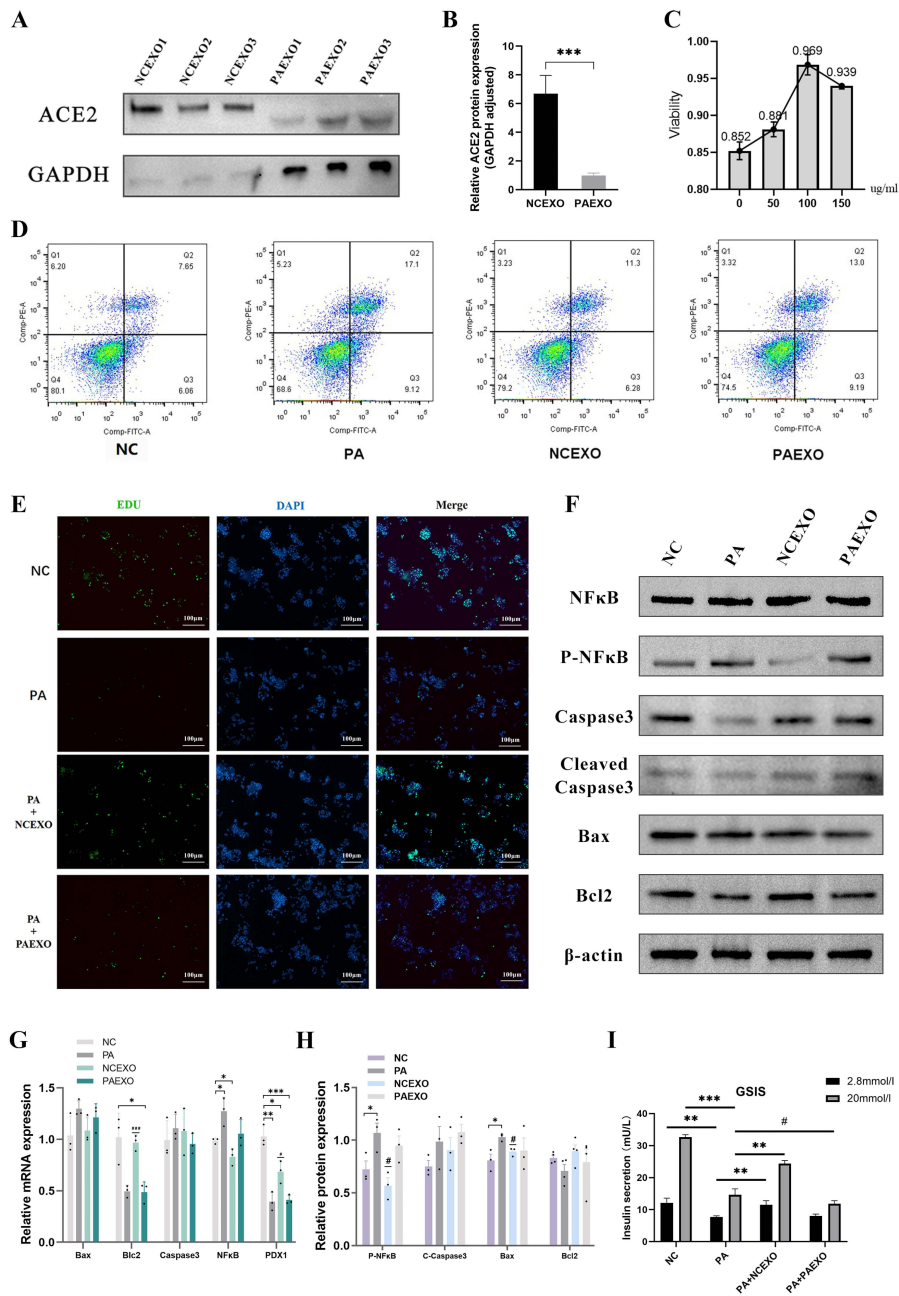


**Figure 2** ACE2-rich NCEXO regulates proliferation, apoptosis and inflammation of islets β-cells in vitro. **(A and B)** WB analysis revealed that NCEXO exhibited higher levels of ACE2 compared to PAEXO. **(C)** Viability assessment of Min6 cells under varying concentrations of exosomes using CCK-8. **(D)** Flow cytometry analysis of Min6 cells apoptosis rate. Unit (%) **(E)** Min6 cell proliferation was determined with an EDU Kit. Bar = 100μm **(F and H)** Protein expression of Bax, Bcl-2, Caspase-3, Cleaved Caspase-3, NFκB and P- NFκB in MIN6 cells and densitometric quantification. **(G)** Real-time PCR analysis of Bax, Bcl-2, Caspase-3, NFκB, PDX1 of Min6 cell. **(I)** Min6 cell insulin secretion ability was measured by GSIS. \*P < 0.05, \*\*P < 0.01 and \*\*\*P < 0.001; #P < 0.05 NCEXO group vs PA group.

population of cells in late-stage apoptosis. Intriguingly, concomitant intervention with NCEXO demonstrated a notable amelioration in the apoptosis rate of Min6 cells during the same conditions(Figure 2D). Subsequently, we examined the impact of exosomes on the proliferation and apoptosis of Min6 cells. EDU assays demonstrated that following 48h of PA treatment, there was a notable decrease in the proliferative capacity of Min6 cells. However, intervention with NCEXO mitigated the impact of PA on Min6 cell proliferation levels. Conversely, the intervention with PAEXO did not yield significant alterations (Figure 2E, Supplementary Figure 1A). In addition, assessment of transcriptional and protein levels provided further evidences of NCEXO’s effect on Min6 cell apoptosis (Figure 2F-H). The results of PCR indicate that



intervention with NCEXO significantly increases the levels of the anti-apoptotic gene Bcl-2 and reduces the expression of NF $\kappa$ B and the pro-apoptotic gene Bax under lipotoxic conditions. Simultaneously, NCEXO intervention upregulates the suppressed PDX1 expression induced by HFD (Figure 2G). WB also demonstrate a significant reduction in p-NF $\kappa$ B and a decrease in the activation of the apoptotic-related protein caspase-3 after NCEXO intervention (Figure 2F and H). In vitro GSIS experiments also revealed that NCEXO could enhance insulin secretion in Min6 cells. However, since NCEXO treatment not only preserves the proliferative ability of Min6 cells but also reduces Min6 cell death induced by PA treatment, it remains uncertain whether the observed enhancement in Min6 cell function is attributed to improved cellular functionality or the increases in cell number(Figure 2I).

## Administration of NCEXO Exhibited the Capacity to Enhance Mice Metabolic Status and $\beta$ -Cell Function

In order to comprehend the in vivo effects of NCEXO and PAEXO, as well as the role and mechanisms of ACE2 within NCEXO, a sequence of animal experiments was conducted (Figure 3A). HFD treated mice not only exhibited notable increases in body weight but also manifested a range of metabolic disturbances. However, upon administering NCEXO at week 12 of HFD, significant reductions in body weight were observed in mice, accompanied by improvements in FBG, insulin sensitivity, and glucose tolerance. In contrast, intervention with PAEXO did not show discernible amelioration of the metabolic disruptions induced by HFD (Figure 3B-G). Studies have demonstrated that metabolic stress induced by HFD results in pronounced hyperinsulinemia and inflammatory responses in mice.<sup>34,35</sup> Consequently, we assessed the serum levels of insulin and IL-1 $\beta$  in mice. Notably, following NCEXO treatment, a significant reduction in serum insulin and IL-1 $\beta$  levels was observed in mice. However, treatment with PAEXO did not show significant improvements in these parameters (Figure 3H-I). Ex vivo GSIS experiments also revealed that HFD treatment increased insulin secretion, while NCEXO could decrease the oversecreted insulin induced by HFD (Figure 3J). This result is also consistent with the hyperinsulinemia in vivo.

The in vitro experiments before have substantiated the pancreas as one of the target organs for NCEXO/PAEXO (Figure 1E and F). Accordingly, we evaluated islets function and morphology. Morphological assessments indicated that both mice on a high-fat diet and mice treated with PAEXO exhibited disrupted cellular arrangement within the islets. Besides, the lipid droplet deposition could be found in HFD group. Conversely, following NCEXO treatment, the islet morphology in mice displayed restored orderly cell arrangement (Figure 3k). The islets constitute approximately 10%–20% of the entire pancreatic blood supply, and the homeostasis of islet microcirculation is important for their function. Therefore, we performed immunohistochemical staining for CD34 and CD31 to assess the state of islet microcirculation. Our findings revealed that mice in the HFD group and the PAEXO group exhibited features such as vascular thickening and neovascularization within the islet vasculature, consistent with previous reports.<sup>36</sup> Notably, NCEXO treatment alleviated vascular dilation and reduced the occurrence of abnormal angiogenesis within the islets (Figure 3L).

## NCEXO Treatment Improved the $\beta$ -Cell Function by Attenuating the Activation of NLRP3 Inflammasomes

To ascertain whether NCEXO/PAEXO treatment impacts  $\beta$ -cell function, we conducted further assessments of crucial transcription factors PDX1 and NKX6.1, pivotal for  $\beta$ -cell functionality. Notably, in mice from both the HFD and PAEXO groups, expression levels of these factors were significantly reduced, while the NCEXO-treated group exhibited a restoration of expression (Figure 4A, B and [Supplementary Figure 1B-1C](#)). In addition, the expression of ACE2 also exhibited a noticeable increase following administration of exogenous ACE2-rich NCEXO. However, in both the HFD and PAEXO groups, ACE2 expression was significantly diminished (Figure 4C, [Supplementary Figure 1D](#)), consistent with the previously observed decline in ACE2 expression induced by the high-fat diet.<sup>9</sup> Moreover, the proportion of  $\alpha$  and  $\beta$  cells in the NCEXO-treated group did not exhibit a significant increase (Figure 4D, [Supplementary Figure 1E-1G](#)), indicating that the intervention of NCEXO confers a certain degree of protective effect on  $\beta$ -cell function. Given that lipid toxicity can induce sustained islets inflammation and NF $\kappa$ B is significantly elevated in cell experiments, we assessed inflammation-related markers and macrophage polarization. The results revealed that NCEXO is capable of ameliorating islets inflammation levels and promoting M2

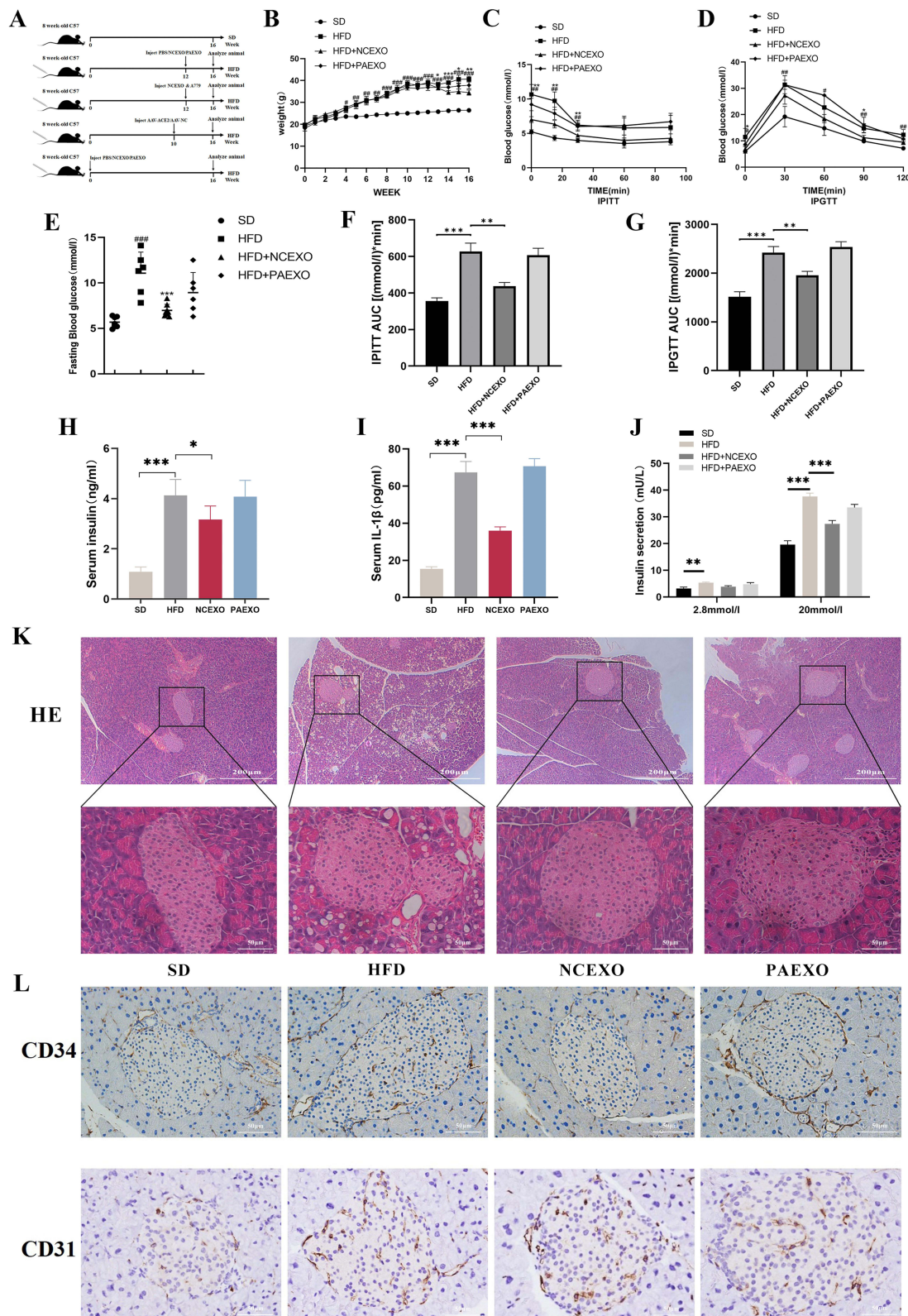


**Figure 3** The metabolic status and  $\beta$ -cell function of NCEXO/PAEXO treated mice. **(A)** Experimental schedule. **(B)** Body weight. **(C)** IPITT and **(D)** IPGTT. **(E)** FBG of mice at week 16 after fasting overnight. AUC of IPITT **(F)** and IPGTT **(G)**. **(H)** Serum insulin and **(I)** L-I $\beta$  measured by Elisa Kits. **(J)** GSIS of primary islets isolated from NC, HFD, NCEXO and PAEXO mice. **(K)** HE images and **(L)** CD31, CD34 immunohistochemical staining of pancreatic islets. Bar = 200 $\mu$ m and Bar = 50 $\mu$ m. ( $^{\#}P < 0.05$ ,  $^{\#\#}P < 0.01$  and  $^{\#\#\#}P < 0.001$  HFD group vs SD group;  $^*P < 0.05$ ,  $^{**}P < 0.01$  and  $^{***}P < 0.001$  NCEXO group vs HFD group in **(B-E)**).

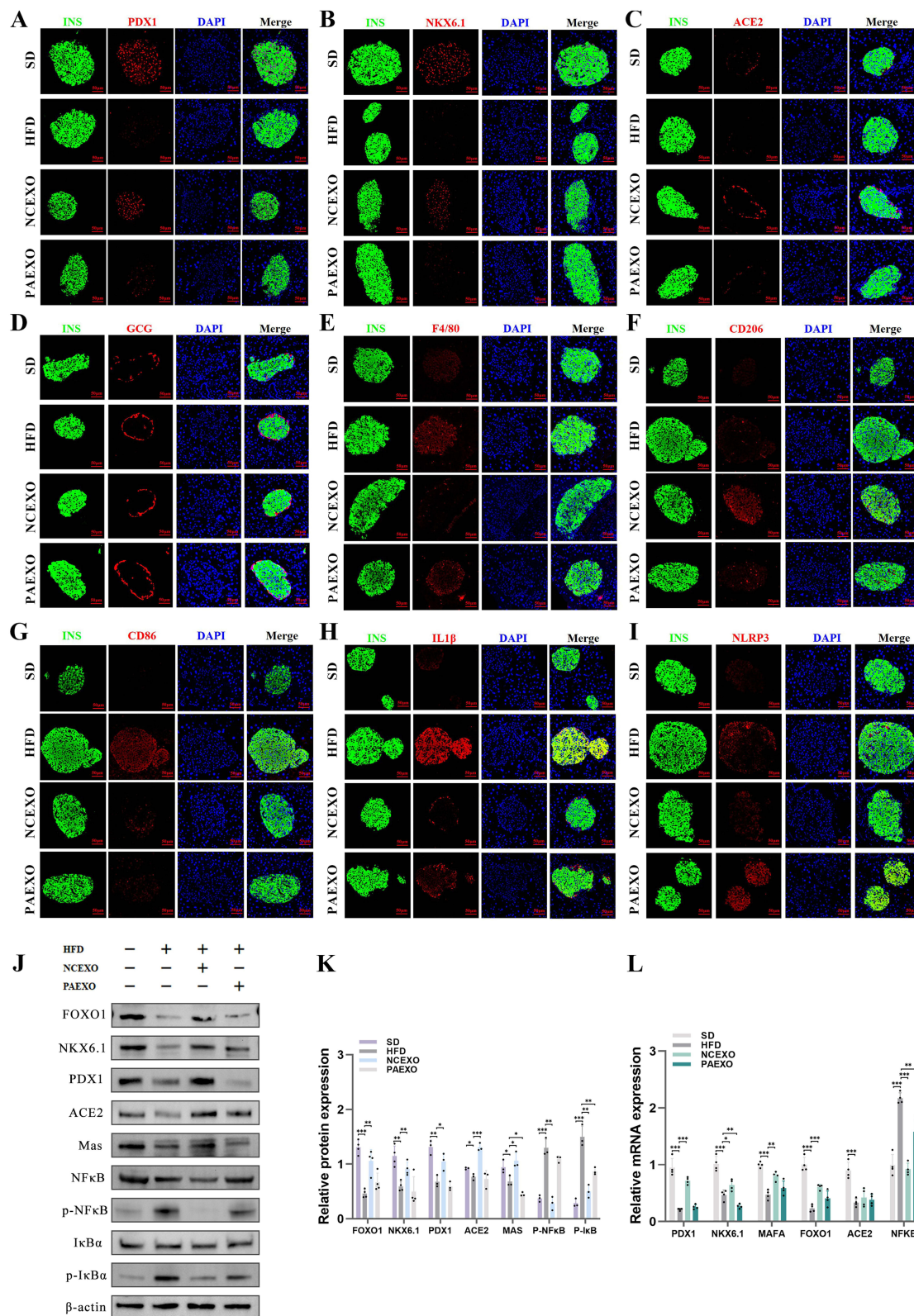


**Figure 4** NCEXO treatment improved the  $\beta$ -cell function by inhibiting the activation of NLRP3 inflammasomes. **(A-I)** Representative double-stained images of insulin and PDX1, insulin and NKX6.1, insulin and ACE2, insulin and glucagon, insulin and F4/80, insulin and CD206, insulin and CD86, insulin and IL1 $\beta$ , insulin and NLRP3. Bar = 50 $\mu$ m **(J and K)** Protein expression of FOXO1, NKX6.1, PDX1, ACE2, Mas, I $\kappa$ B, P-I $\kappa$ B, NF $\kappa$ B and P- NF $\kappa$ B in mouse pancreatic islets and densitometric quantification. **(L)** Quantitative Real-time PCR was used to measure the level of FOXO1, NKX6.1, PDX1, ACE2, NF $\kappa$ B, MAFA of mouse pancreatic islets. \*P < 0.05, \*\*P < 0.01 and \*\*\*P < 0.001.

polarization of macrophages, thereby exerting anti-inflammatory effects. While there was a significant increase in the number of macrophages, the M1 pro-inflammatory state was more pronounced in the HFD group (Figure 4E-H, [Supplementary Figure 1H-IJ](#)). Simultaneously, validation at the transcriptional and protein levels aligns with these findings (Figure 4J-L). Prior research has demonstrated that metabolic stress induced by a high-fat diet leads to islets inflammation and down-regulation of ACE2 expression. Notably, the diminished ACE2 expression disrupts the ACE2/Ang(1–7)/Mas pathway, subsequently attenuating its inhibitory effect on NFκB.<sup>24</sup> This culminates in heightened NFκB expression, thereby triggering the activation of NLRP3 inflammasomes and consequent cellular pyroptosis.<sup>25,37</sup> Existing studies have established a correlation between NLRP3 inflammasome activation and islets function, as well as the progression of diabetes.<sup>16,38,39</sup> In order to delve deeper into potential factors contributing to impaired islets β-cell function and elucidate the mechanisms underlying NCEXO's protective effects, we used immunofluorescence to assess the expression of NLRP3 inflammasomes within the islets. Notably, mice subjected to a high-fat diet and those treated with PAEXO exhibited markedly elevated NLRP3 expression within the islets, whereas in comparison to the HFD group, mice in the NCEXO treatment group displayed a significant reduction in NLRP3 expression (Figure 4I, [Supplementary Figure 1K](#)). Validation through WB and qPCR further confirmed that high-fat diet and PAEXO-treated mice showed substantial activation of NLRP3 inflammasome within the islets, triggering the activation of Caspase-1 and GSDMD, subsequently causing cell pyroptosis (Figure 5A-D).

## The Inhibition of Inflammasome Activation by NCEXO Primarily Stems from Its Abundant ACE2

We identified the higher levels of ACE2 in NCEXO compared to PAEXO (Figure 2A). To determine whether NCEXO's inhibition of inflammasome activation is attributed to its contained ACE2, we performed interventions with Mas receptor blocker A779 and Ang(1–7) analogue A1-7 in Min6 cells. Remarkably, even under lipotoxicity and despite PAEXO intervention, A1-7 partially restored the proliferative capacity of Min6 cells (Figure 5F, [Supplementary Figure 1L](#)). However, the co-intervention of protective NCEXO and A779 resulted in a substantial attenuation of NCEXO's protective effect. This not only significantly diminished the proliferative capacity of Min6 cells but also exacerbated islets function impairment and increased inflammation levels (Figure 5E-I). Thereafter, examination of inflammasome associated signaling molecules in the various groups of cells revealed that A1-7 intervention exerted a positive effect, evident at both protein and transcriptional levels. On the other hand, upon antagonizing the ACE2/Ang(1–7)/Mas pathway with A779, the action of exosomal ACE2 was hindered, resulting in inflammasome activation and cellular pyroptosis (Figure 5C, G and H).

In animal experiments, we administered A779 via intraperitoneal injection in mice to explore variations in NCEXO's effects. Additionally, ACE2<sup>ko</sup> mice were generated to further confirm the crucial role of ACE2 within NCEXO. Regardless of whether the mice WT or ACE2<sup>ko</sup>, after 16 weeks of HFD feeding, their body weight, FBG, IPITT, and IPGTT were significantly elevated compared to their respective SD control groups. However, following 4 weeks of intervention with ACE2-rich NCEXO, notable improvements in metabolic status were observed in both WT and ACE2<sup>ko</sup> mice. However, this amelioration could be counteracted by treatment of A779 (Figure 6A-F). Notably, even with A779 intervention, there was still an improvement in metabolic status compared to the HFD group. NCEXO also demonstrated significant protective effects in ACE2<sup>ko</sup> mice subjected to HFD. It not only enhanced the expression of FOXO1, NKX6.1, and PDX1 but also reduced the expression of inflammation-related molecules and cellular pyroptosis caused by NLRP3 activation. However, A779 intervention markedly attenuated NCEXO's protective effects (Figure 6G-I). Similarly, the hyperinsulinemia and elevated inflammation levels induced by HFD could be significantly ameliorated with NCEXO intervention. However, concurrent administration of A779 resulted in notably higher levels of hyperinsulinemia and inflammation compared to the NCEXO group (Figure 6J and K). Finally, at the histological level of mouse islets, the results revealed that islet cells in WT mice on a high-fat diet displayed disorganized arrangement and visible vascular thickening. Following NCEXO intervention, islet morphology showed improvement, while A779 intervention exacerbated islets damage. In ACE2<sup>ko</sup> mice subjected to HFD, the islets suffered severe damage, characterized by disrupted cellular arrangement and evident islets cell loss. However, NCEXO treatment led to improvement of islets damage in ACE2<sup>ko</sup> mice (Figure 7A). Immunofluorescence further indicated that ACE2<sup>ko</sup> mice, deprived of ACE2 protection, were

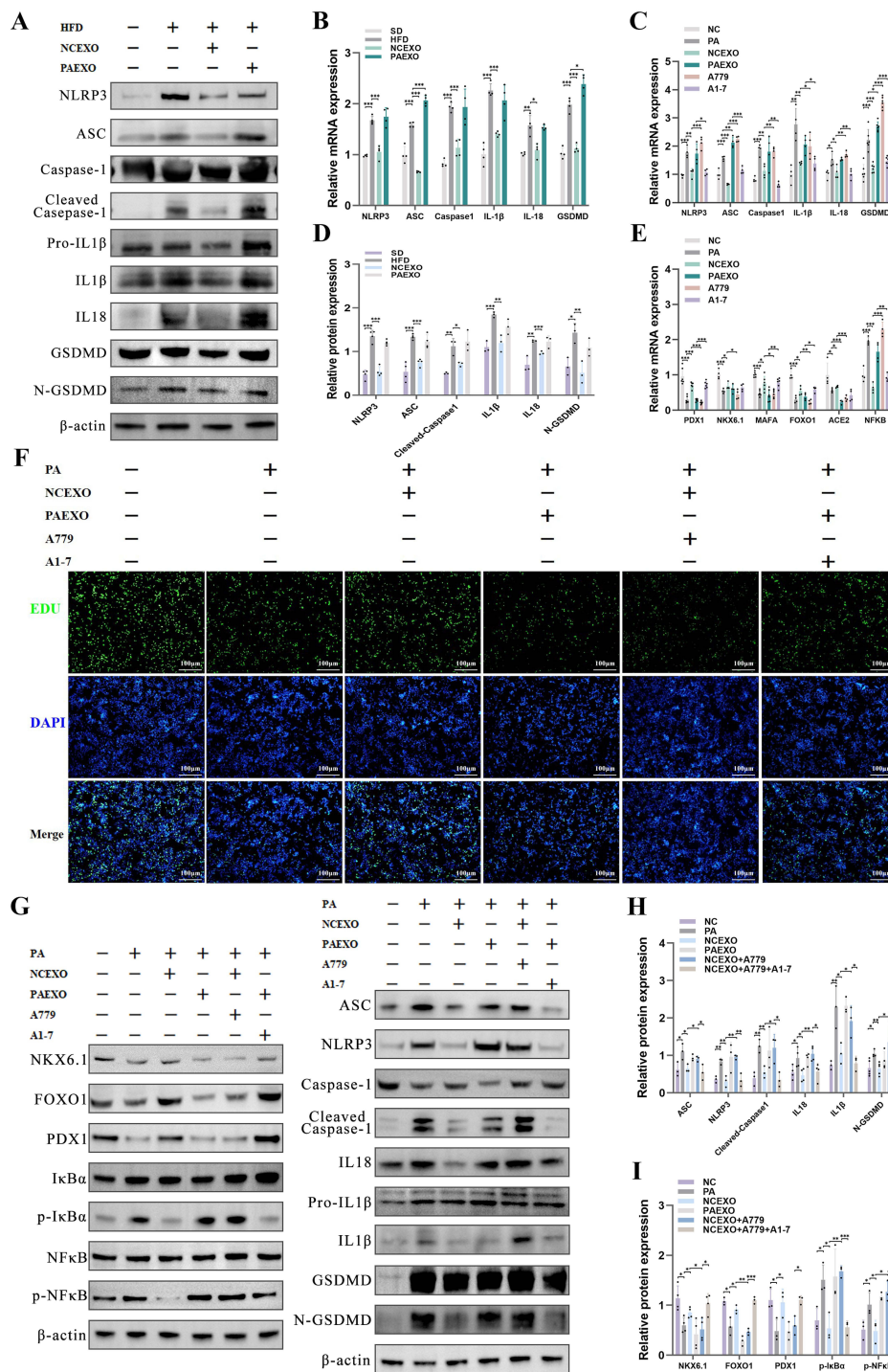


**Figure 5** The protective effect of NCEXO primarily stems from its ACE2. **(A)** Protein expression of NLRP3, ASC, Caspase-1, Cleaved Caspase-1, Pro-IL $\beta$ , IL1 $\beta$ , IL18, GSDMD and N- GSDMD in mouse pancreatic islets and densitometric quantification. **(B)** Quantitative Real-time PCR was used to measure the level of NLRP3, ASC, Caspase-1, IL1 $\beta$ , IL18, GSDMD of mouse pancreatic islets. **(C)** Quantitative Real-time PCR was used to measure the level of NLRP3, ASC, Caspase-1, IL1 $\beta$ , IL18, GSDMD of mouse pancreatic islets. **(D)** The densitometric quantification of Protein expression of NLRP3, ASC, Caspase-1, Cleaved Caspase-1, Pro-IL $\beta$ , IL1 $\beta$ , IL18, GSDMD and N- GSDMD in mouse pancreatic islets. **(E)** Quantitative Real-time PCR was used to measure the level of FOXO1, NKX6.1, PDX1, ACE2, NF $\kappa$ B, MAFA of Min6 cell. **(F)** Effect of A779/A1-7 on Min6 cells proliferation measured by EDU. Bar = 100 $\mu$ m **(G-I)** Protein expression of FOXO1, NKX6.1, PDX1, I $\kappa$ B, P-I $\kappa$ B, NF $\kappa$ B, P- NF $\kappa$ B, NLRP3, ASC, Caspase-1, Cleaved Caspase-1, Pro-IL $\beta$ , IL1 $\beta$ , IL18, GSDMD and N- GSDMD in Min6 cell. \*P < 0.05, \*\*P < 0.01 and \*\*\*P < 0.001.

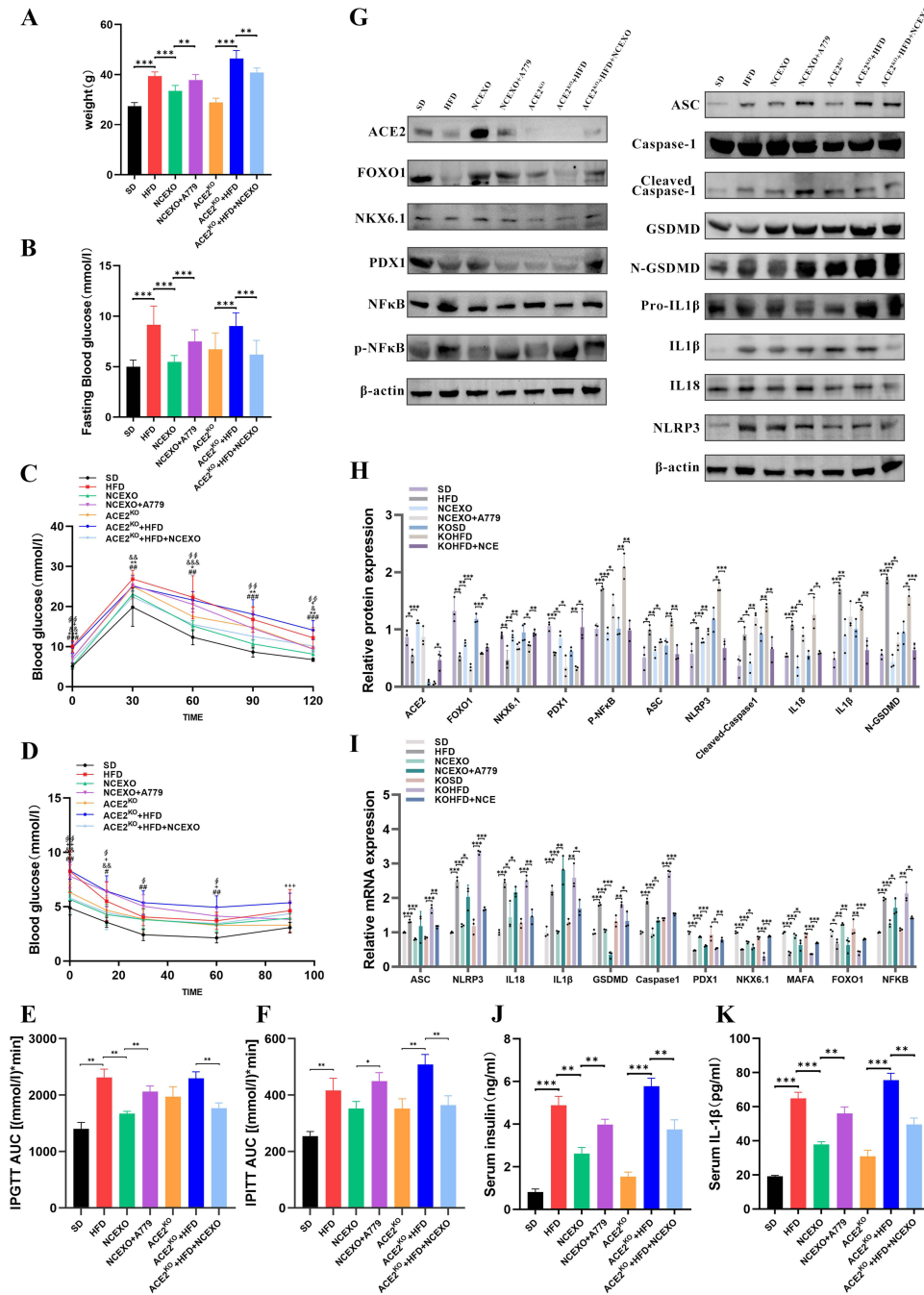


**Figure 6** NCEXO reduced the damage caused by HFD both in WT and ACE2<sup>KO</sup> mice. **(A)** Body weight. **(B)** FBG. **(C)** IPGTT and **(D)**IPITT. (<sup>#</sup>P < 0.05, <sup>###</sup>P < 0.001 HFD group vs SD group; <sup>\*</sup>P < 0.05, <sup>\*\*</sup>P < 0.01 and <sup>\*\*\*</sup>P < 0.001 NCEXO group vs HFD group; <sup>&</sup>P < 0.05, <sup>&&</sup>P < 0.01 and <sup>&&&</sup>P < 0.001 NCEXO+A779 group vs NCEXO group; <sup>†</sup>P < 0.05, <sup>††</sup>P < 0.01 and <sup>†††</sup>P < 0.001 ACE2<sup>KO</sup> vs ACE2<sup>KO</sup>+HFD group; <sup>§</sup>P < 0.05, <sup>§§</sup>P < 0.01 ACE2<sup>KO</sup>+HFD group vs ACE2<sup>KO</sup>+HFD+NCEXO group in **(C)** and **(D)**). AUC of IPGTT(**E**) and IPITT(**F**) of mice at week 16 after fasting overnight. **(G)** and **(H)** Protein expression of ACE2, FOXO1, NKX6.1, PDX1, NFκB, P- NFκB, NLRP3, ASC, Caspase-1, Cleaved Caspase-1, Pro-IL1β, IL1β, IL18, GSDMD and N- GSDMD in mouse pancreatic islets. **(I)** Quantitative Real-time PCR was used to measure the level of FOXO1, NKX6.1, PDX1, NFκB, MAFA, NLRP3, ASC, Caspase-1, IL1β, IL18, GSDMD of mouse pancreatic islets. **(J)** Serum insulin and **(K)**IL-1β measured by Elisa Kits. <sup>\*</sup>P < 0.05, <sup>\*\*</sup>P < 0.01 and <sup>\*\*\*</sup>P < 0.001.

more susceptible to lipotoxicity, intensifying inflammasome activation and cellular pyroptosis within the islets. This ultimately led to impaired islets function and islet cell loss. Notably, ACE2-riched NCEXO demonstrated a protective effect in both HFD WT and ACE2<sup>KO</sup> mice (Figure 7B-G, Supplementary Figure 2A-2H).

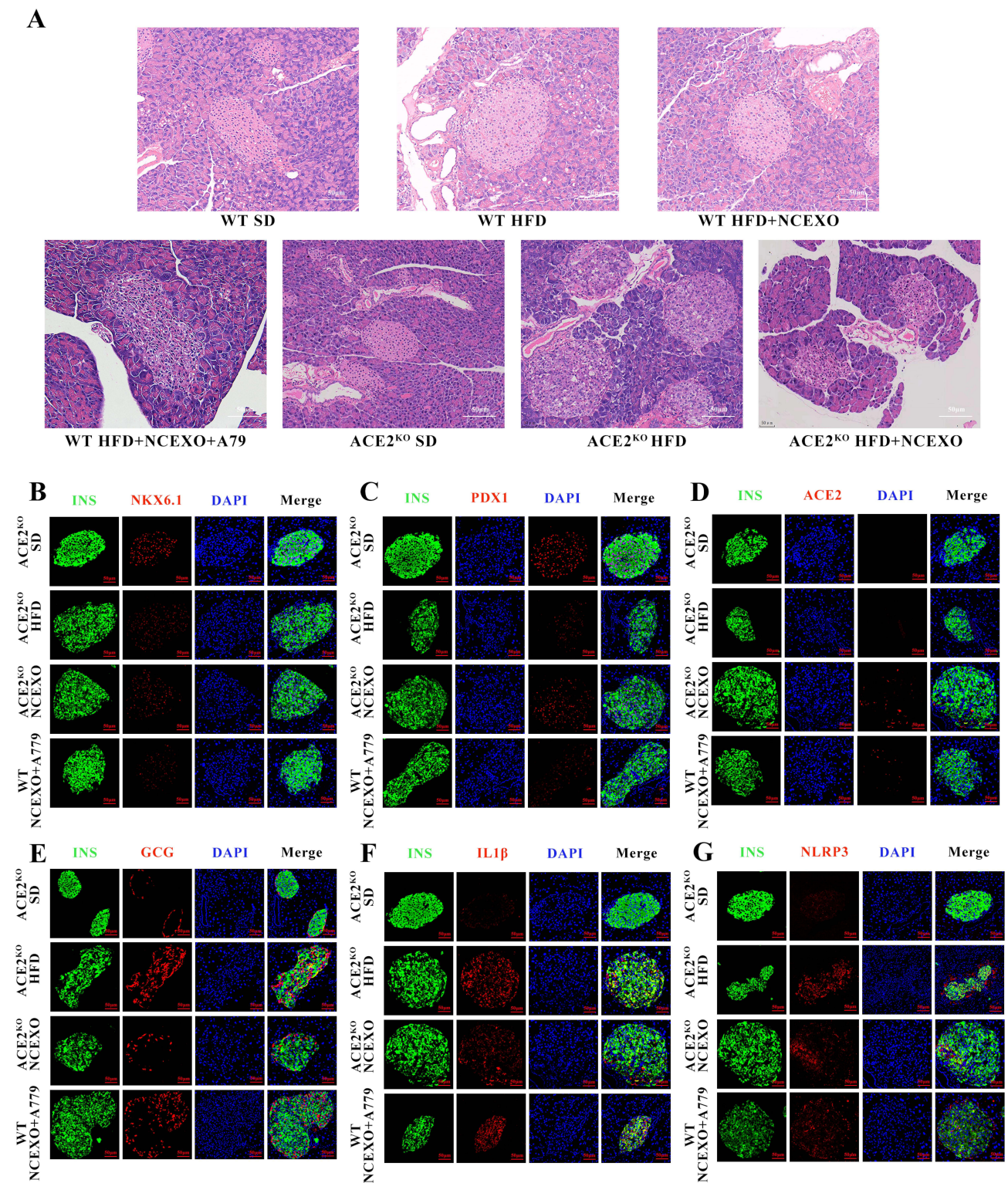


**Figure 7** Islets  $\beta$  cell morphology analysis in WT and ACE2<sup>ko</sup> mice. **(A)** HE images and **(B-G)** representative double-stained images of insulin and PDX1, insulin and NKX6.1, insulin and ACE2, insulin and glucagon, insulin and IL1 $\beta$ , insulin and NLRP3. Bar = 50 $\mu$ m.

## Early Preventative Treatment of NCEXO Improves the Metabolic Status of HFD Mice

Prevention of disease holds greater significance than treatment. To explore whether NCEXO can exert its effects in the early prevention of metabolic disturbances, we performed early 24-hour PA interventions *in vitro* to assess apoptosis rate.

Remarkably, after 24 hours of PA treatment, apoptosis predominantly occurred in the Q3 quadrant ([Supplementary Figure 3A](#)), indicating an early-stage apoptosis, distinct from the primarily observed late-stage apoptosis after 48 hours of treatment ([Figure 2C](#)). NCEXO intervention led to a notable reduction in the proportion of cell apoptosis compared to the PA group. This suggests that NCEXO can provide a certain degree of protection to Min6 cells against lipotoxicity in the early stages ([Supplementary Figure 3A](#)). In subsequent *in vivo* experiments, we began intravenous injections of NCEXO and PAEXO to mice from the first week of HFD. The results also demonstrated that early NCEXO intervention led to significant improvements in mouse body weight, FBG, IPITT, IPGTT, serum insulin levels, and serum IL-1 $\beta$  levels ([Supplementary Figure 3B-3J](#)). Although food intake in the NCEXO group appeared to decrease compared to the HFD group, the results were not statistically significant ([Supplementary Figure 3F](#)). It is noteworthy that early intervention with PAEXO also showed improvements in mouse metabolic levels.

Furthermore, to compare the therapeutic effects of NCEXO with those of ACE2 overexpression, we administered interventions of NCEXO, AAV-NC, and AAV-ACE2 separately to mice of HFD, followed by a 4-week period. Notably, while the reduction in FBG was similarly observed in both groups, NCEXO demonstrated superior effects over AAV-ACE2 in terms of reducing mouse body weight, serum insulin, serum IL-1 $\beta$ , IPITT, and IPGTT levels ([Supplementary Figure 3K-3S](#)). Finally, to preliminarily explore the reasons behind the discrepancy in ACE2 content between NCEXO and PAEXO, we conducted immunofluorescence experiments in mouse small intestinal tissue. Remarkably, compared to SD mice, ACE2 expression within the small intestine of mice after 16 weeks of high-fat diet feeding showed a significant reduction ([Supplementary Figure 3Q](#), [Supplementary Figure 2I](#)). While existing reports indicate that lipid toxicity can disrupt the intestinal barrier and lead to gut damage,<sup>40</sup> potentially affecting the secretion of exosomes, the substantial downregulation of ACE2 expression is likely one of the key factors contributing to the significant decrease in ACE2 content within PAEXO.

## Discussion

In recent years, with the deepening exploration of gut microbiota and gut endocrine hormones, the relationship between the intestine and the islets has gradually come to light. The discovery and application of gut-derived factors like GLP-1 and GIP have propelled the “gut-islet axis” theory into a prominent focus of research attention. The “gut-islet axis” represents a crucial endocrine signaling pathway through which gut microbiota and endocrine metabolism regulate islets function. Through extensive investigation into gut microbiota, it has been found that gut-derived exosomes containing microbial DNA can accumulate in islets  $\beta$  cells of obese mice, inducing inflammation and impairing  $\beta$  cell function.<sup>6</sup> This underscores the potential of gut-derived exosomes to exert biological effects remotely on islets, revealing a significant latent capacity for regulating islets function. The discovery and long-range regulatory effects of gut-derived exosomes have further enriched the scope of gut endocrine and “gut-islet axis” regulation theories, revealing substantial opportunities for extensive research in this field.

Our study revealed significant differences in ACE2 content between NCEXO and PAEXO, potentially attributed to a notable reduction in ACE2 expression in intestinal endocrine cells under conditions of lipotoxicity ([Supplementary Figure 3Q](#)). However, NTA results demonstrated that the particle concentration of NCEXO was 2.71 E+10 particles/mL, while that of PAEXO reached 2.71 E+12 particles/mL ([Figure 1C](#)), indicating that cells undergoing reduced cell count due to lipotoxicity and hyperglycemic damage secrete a higher amount of exosomes. Prior to the discovery that exosomes contain nucleic acids, proteins, and other substances, exosomes were generally regarded as a means for cells to clear metabolic waste. Thus, we speculate that intestinal endocrine cells affected by lipotoxicity might generate more toxic substances or metabolic waste, such as reactive oxygen species. Increased exosome secretion could potentially be a protective mechanism of the cells to enhance the clearance of harmful materials. This explanation partially elucidates why the introduction of PAEXO in both *in vitro* and *in vivo* experiments leads to adverse outcomes, as adding PAEXO might accelerate the accumulation of detrimental substances within the cells. However, further validation of this hypothesis is required, particularly in terms of identifying the bioactive substances within NCEXO and PAEXO. Similarly, the targeting specificity of exosomes is also a topic of interest. Our experiments indicated that after tail vein injection of PKH67-labeled exosomes, abundant exosome aggregates were detected not only in the pancreas but also in the liver of mice. However, exosome aggregates were not detected in other organs such as the kidneys and intestines (data not show), suggesting different organ targeting *in vivo* of exosomes with different cellular origins.



In this study, we found abundant expression of ACE2 in the exosomes secreted by small intestinal endocrine cells. The classical understanding of ACE2 primarily revolves around its role as a crucial component of the renin–angiotensin system (RAS), functioning in opposition to the ACE signaling pathway as a key element of the ACE2/Ang1-7/Mas axis. This axis has garnered significant attention due to its dual effect, reminiscent of both ACE inhibitors (ACEIs) and angiotensin receptor blockers (ARBs), as it not only reduces the levels of angiotensin II (Ang II) but also antagonizes its effects.<sup>41</sup> Recent research has revealed the complete presence of the ACE2/Ang1-7/Mas axis within islets tissue, contributing to localized islets regulation. ACE2 operates through Mas receptors, enhancing pancreatic microcirculation, safeguarding endothelial cell function, and concurrently inhibiting oxidative stress and inflammatory reactions. Consequently, ACE2 counters the dedifferentiation of pancreatic  $\beta$ -cells under metabolic stress, positively modulating their function and differentiation status, and promoting  $\beta$ -cell proliferation.<sup>9,10</sup> Furthermore, ACE2 is widely distributed within the intestinal tract, with its highest expression in the small intestine. In this context, it serves beneficial roles, including anti-inflammatory, immunomodulatory, and barrier-maintaining functions, thus contributing to intestinal homeostasis. Notably, viral infections and inflammatory states significantly decrease ACE2 expression in the intestines, impairing its protective functions and leading to compromised intestinal barrier integrity and heightened susceptibility to inflammation,<sup>42,43</sup> this observation aligns with our findings of significantly reduced ACE2 expression in the intestines of high-fat diet mice. This indicates that ACE2 may regulate islets cell function through both local islets and “gut-islets axis” pathways. However, the role of ACE2 mediated by intestinal exosomes in the regulation of pancreatic cell function, as a novel component of the “gut-islets axis”, and its underlying molecular mechanisms remain relatively unexplored. Our findings suggest that ACE2, in addition to its local regulatory role between the intestines and the islets, operates through a novel pathway and mechanism—mediated by intestinal exosomes—to influence distal islets function. This establishes a new link for interplay between the intestine and the islets, forming a novel avenue for the “gut-islets axis” regulation. Consequently, it enriches the regulatory framework of the “gut-islets axis” theory with new insights.

The NLRP3 inflammasome consists of a sensor (NLRP3), an adapter (ASC, also known as PYCARD), and an effector (caspase-1). NLRP3 detects a broad range of microbial motifs, endogenous danger signals and environmental irritants, resulting in the formation and activation of the NLRP3 inflammasome. Activation of the NLRP3 inflammasome leads to caspase-1-dependent release of IL-1 $\beta$  and IL-18, as well as GSDMD-mediated pyroptosis. We observed NLRP3 activation and pyroptosis after 48 hours of PA stimulation and 16 weeks of high-fat diet feeding. Moreover, in ACE2<sup>ko</sup> mice, islets exhibited more pronounced cellular pyroptosis, and immunofluorescence revealed extracellular leakage of NLRP3 around the islets (Figure 7G). This suggests excessive formation of pores by GSDMD-N due to heightened pyroptosis, leading to cell swelling and rupture, with intracellular NLRP3 either utilizing the pores generated by GSDMD-N or being released extracellularly upon cell rupture. In contrast, pyroptosis was less severe in islets of HFD-fed WT mice, indicating that ACE2 deficiency accelerated the progression of cellular pyroptosis. It is worth noting that the results of the cell apoptosis experiments differed between the 24-hour (Supplementary Figure 3A) and 48-hour (Figure 2C) PA stimulations. Following the short-term 24-hour intervention, early apoptosis in the Q3 quadrant was prominent in Min6 cells, while after the 48-hour intervention, late apoptosis in the Q2 quadrant was predominant. Our apoptosis detection method, based on Annexin V, shares mechanistic similarities with both cell pyroptosis and late-stage apoptosis,<sup>20</sup> which means Annexin V cannot differentiate apoptotic cells from pyroptotic cells. Therefore, the cell population detected after 48-hour PA stimulation likely encompasses both cells undergoing late-stage apoptosis and those undergoing pyroptosis. This observation also suggests that the initiation of cell pyroptosis has not yet occurred following 24-hour PA stimulation, underscoring the critical importance of early intervention and preventive measures. Another point of significance is that the composition and functions of exosomes can vary with changes in cellular or intracellular environments. Not only can viral infections and pro-inflammatory cytokines alter the molecular composition of exosomes,<sup>44</sup> but also in type 2 diabetes patients, plasma exosome components exhibit notable changes following blood glucose control therapy.<sup>45</sup> Therefore, in individuals with metabolic syndrome or diabetes undergoing hypoglycemic treatment, could the composition of exosomes released by their intestinal endocrine cells change? If not, should protective or reparative strategies for the intestine be considered in their treatment regimen? These questions need in-depth research and exploration.

The current focus on exosomes extends beyond their value as carriers for therapeutic agents; the inherent therapeutic potential of exosomes from various cell sources is equally significant. With characteristics such as strong biocompatibility, minimal rejection, and tunability, exosomes have become an ideal treatment approach.<sup>46</sup> Our study indicates that intravenous injection of NCEXO enriched with ACE2 in HFD mice led to weight reduction and improved metabolism. Additionally, NCEXO's targeting of pancreatic islets provides insights and value for addressing metabolic syndrome and diabetes treatments. However, a current challenge is the low yield of exosomes. Sustaining the required exosome dosage for animal experiment demands continuous cell cultivation, intervention, and extraction, entailing notable costs. Moreover, determining exosomes utilization and optimal concentrations in vivo remains challenging. Dosage determination for therapeutic agents presents difficulties, as does evaluating the administration route—intravenous injection or targeted pancreatic islet injection. These aspects necessitate further exploration in our subsequent research endeavors.

This study has certain limitations. I. Although differences were observed in the extracted ACE2 content of the two types of exosomes, little is known about differences in their other components or the biological active substances they contain. II. While the exosome dosage for in vivo experiments was referenced from previous literature summaries,<sup>47</sup> the extended duration of the high-fat animal model prevented further determination of the optimal in vivo dosage and dosing frequency. III. Although  $\beta$  cells are of utmost importance within islets, the potential effects of NCEXO and PAEXO on  $\alpha$  cells and vascular endothelial cells remain unclear. While immunofluorescence indicates that NCEXO can improve the ratio of  $\alpha$  cells to  $\beta$  cells in the pancreatic islets of HFD mice, as well as enhance islet microcirculation, it is yet to be confirmed whether NCEXO directly affects  $\alpha$  cells and vascular endothelial cells.

In conclusion, our study demonstrates that ACE2-enriched intestinal-derived exosomes(NCEXO) can selectively target pancreatic islets and provide partial protection against lipotoxicity-induced damage to  $\beta$  cells. This protective effect primarily involves the activation of the ACE2/Ang(1–7)/Mas pathway, which in turn regulates NF $\kappa$ B expression, thereby inhibiting NLRP3 inflammasome activation and cellular pyroptosis. Our findings highlight the unique role of exosomes in the regulation of the “gut-islet axis”, providing a new direction for the treatment of diabetes and metabolic syndrome.

## Abbreviations

ACE2, Angiotensin-converting enzyme 2; ACE2<sup>ko</sup>, ACE2 knockout; ACEI, Angiotensin-converting enzyme inhibitor; AAV, Adeno-associated virus; ALIX, Apoptosis-linked gene 2-interacting protein X; A1-7, Angiotensin 1-7; A779, Mas receptor blocker A779; AngII, Angiotensin II; ARB, Angiotensin Receptor Blockers; ASC, apoptosis-associated speck-like protein; Bcl-2, B-cell lymphoma-2; Bax, BCL2-Associated X; BSA, Bovine serum albumin; CCK-8, Cell Counting Kit-8; DPP4, Dipeptidyl peptidase IV; EXO, Exosome; ECL, Enhanced chemiluminescence; FBG, Fasting blood glucose; FoxO1, Forkhead box O1; F4/80, EGF-like module-containing mucin-like hormone receptor-like 1; GLP-1, Glucagon-like peptide-1; Gcg, Glucagon; GIP, Gastric Inhibitory Peptide; GSDMD Gasdermin D; GSIS, Glucose-stimulated insulin secretion; HE, Htoxylin eosin; HFD, High-fat diet; IL-1 $\beta$ , Interleukin-1 $\beta$ ; IL-18, Interleukin-18; IPGTT, Intraperitoneal glucose tolerance test; IPITT, Intraperitoneal insulin tolerance test; IR, Insulin resistance; MAfA, Musculus v-maf musculoaponeurotic fibrosarcoma oncogene; family, protein A; NF $\kappa$ B, Nuclear factor kappa-B; NTA, Nanoparticle tracking analysis; I $\kappa$ B, Inhibitor of NF- $\kappa$ B; NKX6.1, NK6 transcription factor related, locus 1; NLRP3, NBD-, LRR- and pyrin domain-containing 3; miRNA, Micro RNA; PA, Palmitic acid; PDX1, Pancreas/duodenum homeobox protein-1; PYCARD, PYD And CARD Domain Containing; qPCR, Quantitative polymerase chain reaction; RAS, Renin–angiotensin system; SD, Standard diet; SPF, Specific pathogen free; T2DM, Type 2 diabetes mellitus; TEM, Transmission electron microscopy; TSG101, Tumor susceptibility gene 101; WB, Western blot; WT, Wild type.

## Data Sharing Statement

The datasets generated during and analyzed during the current study are not publicly available but are available from the corresponding author on reasonable request.

## Consent for Publication

All authors approved the final manuscript and the submission to this journal.

## Funding

This research was funded by National Natural Science Foundation of China, grant number 82170812, 82302878 and 81974104.

## Disclosure

The authors declare no conflict of interest.

## References

1. Rooney MR, Fang M, Ogurtsova K, et al. Global Prevalence of Prediabetes. *Diabetes Care*. 2023;46(7):1388–1394. doi:10.2337/dc22-2376
2. Yang S, Cao J, Sun C, Yuan L. The Regulation Role of the Gut-Islets Axis in Diabetes. *Diabetes Metab Syndr Obes*. 2024;17(1415–1423):1415–1423. doi:10.2147/DMSO.S455026
3. Zhou M, Yu J, Li X, Ruan Z, Yu S. Role of the gut microbiota and innate immunity in polycystic ovary syndrome: current updates and future prospects. *J Cell Mol Med*. 2024;28(8):e18258. doi:10.1111/jcmm.18258
4. Bany Bakar R, Reimann F, Gribble F. The intestine as an endocrine organ and the role of gut hormones in metabolic regulation. *Nat Rev Gastroenterol Hepatol*. 2023;20(12):784–796. doi:10.1038/s41575-023-00830-y
5. Kalluri R, LeBleu VS. The biology, function, and biomedical applications of exosomes. *Science*. 2020;367(6478). doi:10.1126/science.aau6977
6. Gao H, Luo Z, Ji Y, et al. Accumulation of microbial DNAs promotes to islet inflammation and beta cell abnormalities in obesity in mice. *Nat Commun*. 2022;13(1):565. doi:10.1038/s41467-022-28239-2
7. Chen T, Zhang B, He G, et al. Gut-Derived Exosomes Mediate the Microbiota Dysbiosis-Induced Spermatogenesis Impairment by Targeting Meiotic in Mice. *Adv Sci*. 2024.
8. Santos RA-O, Sampaio WO, Alzamora AC, et al. The ACE2/Angiotensin-(1-7)/MAS Axis of the Renin-Angiotensin System: focus on Angiotensin-(1-7). *J Med*. 2018.
9. Xuan X, Gao F, Ma X, et al. Activation of ACE2/angiotensin (1-7) attenuates pancreatic beta cell dedifferentiation in a high-fat-diet mouse model. *Metabolism*. 2018;81:83–96. doi:10.1016/j.metabol.2017.12.003
10. Ma X, Gao F, Chen Q, et al. ACE2 modulates glucose homeostasis through GABA signaling during metabolic stress. *J Endocrinol*. 2020;246(3):223–236. doi:10.1530/JOE-19-0471
11. Chen Q, Gao F, Gao Y, et al. Intestinal ACE2 regulates glucose metabolism in diet-induced obese mice through a novel gut-islet axis mediated by tryptophan. *Obesity*. 2023;31(5):1311–1325. doi:10.1002/oby.23719
12. Chittimalli K, Jahan J, Sakamuri A, McAdams ZL, Ericsson AC, Jarajapu Y. Restoration of the gut barrier integrity and restructuring of the gut microbiome in aging by angiotensin-(1-7). *Clin Sci*. 2023;137(11):913–930. doi:10.1042/CS20220904
13. Hashimoto T, Perlot T, Rehman A, et al. ACE2 links amino acid malnutrition to microbial ecology and intestinal inflammation. *Nature*. 2012;487(7408):477–481. doi:10.1038/nature11228
14. Yu W, Ou X, Liu X, et al. ACE2 contributes to the maintenance of mouse epithelial barrier function. *Biochem Biophys Res Commun*. 2020;533(4):1276–1282. doi:10.1016/j.bbrc.2020.10.002
15. Oliveira LP, Guimarães VHD, Oliveira JR, et al. Genetic deletion of the angiotensin-(1-7) receptor Mas leads to alterations in gut villi length modulating TLR4/PI3K/AKT and produces microbiome dysbiosis. *Neuropeptides*. 2020;82(102056):102056. doi:10.1016/j.npep.2020.102056
16. Schroder K, Zhou R, Fau T, Tschopp J, Tschopp J. The NLRP3 inflammasome: a sensor for metabolic danger? *Science (New York, NY)*. 2010;327(5963):296–300. doi:10.1126/science.1184003
17. Chou WC, Jha S, Linhoff MW, Ting JP. The NLR gene family: from discovery to present day. *Nat Rev Immunol*. 2023;23(10):635–654. doi:10.1038/s41577-023-00849-x
18. Shi J, Zhao Y, Wang K, et al. Cleavage of GSDMD by inflammatory caspases determines pyroptotic cell death. *Nature*. 2015;526(7575):660–665. doi:10.1038/nature15514
19. Ding J, Wang K, Liu W, et al. Pore-forming activity and structural autoinhibition of the gasdermin family. *Nature*. 2016;535(7610):111–116. doi:10.1038/nature18590
20. Yu P, Zhang X, Liu N, Tang L, Peng C, Chen X. Pyroptosis: mechanisms and diseases. *Signal Transduction and Targeted Therapy*. 2021;6(1):128. doi:10.1038/s41392-021-00507-5
21. Broz P, Pelegrin P, Shao F. The gasdermins, a protein family executing cell death and inflammation. *Nat Rev Immunol*. 2020;20(3):143–157. doi:10.1038/s41577-019-0228-2
22. Swanson K, Deng M, Ting J. The NLRP3 inflammasome: molecular activation and regulation to therapeutics. *Nat Rev Immunol*. 2019;19(8):477–489. doi:10.1038/s41577-019-0165-0
23. Bauernfeind FG, Horvath G, Stutz A, et al. Cutting edge: NF-kappaB activating pattern recognition and cytokine receptors license NLRP3 inflammasome activation by regulating NLRP3 expression. *J Immunol*. 2009;183(2):787–791. doi:10.4049/jimmunol.0901363
24. Zhang X, Jia F, Ma W, Li X, Zhou X. DAD3 targets ACE2 to inhibit the MAPK and NF-kappaB signalling pathways and protect against LPS-induced inflammation in bovine mammary epithelial cells. *Vet Res*. 2022;53(1):104. doi:10.1186/s13567-022-01122-0
25. Xu S, Chen H, Ni H, Dai Q. Targeting HDAC6 attenuates nicotine-induced macrophage pyroptosis via NF-kappaB/NLRP3 pathway. *Atherosclerosis*. 2021;317:1–9. doi:10.1016/j.atherosclerosis.2020.11.021
26. Zhao W, Ma L, Cai C, Gong X. Caffeine Inhibits NLRP3 Inflammasome Activation by Suppressing MAPK/NF-kappaB and A2aR Signaling in LPS-Induced THP-1 Macrophages. *Int J Bio Sci*. 2019;15(8):1571–1581. doi:10.7150/ijbs.34211
27. Zhong Z, Umemura A, Sanchez-Lopez E, et al. NF-kappaB Restricts Inflammasome Activation via Elimination of Damaged Mitochondria. *Cell*. 2016;164(5):896–910. doi:10.1016/j.cell.2015.12.057
28. Huang H, Wang J, Liu Z, Gao F. The angiotensin-converting enzyme 2/angiotensin (1-7)/mas axis protects against pyroptosis in LPS-induced lung injury by inhibiting NLRP3 activation. *Arch Biochem Biophys*. 2020;693:108562. doi:10.1016/j.abb.2020.108562

29. You Y, Huang Y, Wang D, et al. Angiotensin (1-7) inhibits arecoline-induced migration and collagen synthesis in human oral myofibroblasts via inhibiting NLRP3 inflammasome activation. *J Cell Physiol.* 2019;234(4):4668–4680. doi:10.1002/jcp.27267
30. Lei S, Chen X, Wu J, Duan X, Men K. Small molecules in the treatment of COVID-19. *Signal Transduction and Targeted Therapy.* 2022;7(1):387. doi:10.1038/s41392-022-01249-8
31. Tiwari V, Singh J, Tiwari P, et al. ACE2/ANG-(1-7)/Mas receptor axis activation prevents inflammation and improves cognitive functions in streptozotocin induced rat model of Alzheimer's disease-like phenotypes. *Eur. J. Pharmacol.* 2023;946:175623. doi:10.1016/j.ejphar.2023.175623
32. Yang S, Zhang J, Zeng T, Zheng J, Min J, Chen L. Role of Circulating Exosomal miRNA-3976 in Early Diabetic Retinopathy. *Int J Nanomed.* 2023;18:3695–3709. doi:10.2147/IJN.S414393
33. Kong L, Zhao Q, Jiang X, et al. Trimethylamine N-oxide impairs beta-cell function and glucose tolerance. *Nat Commun.* 2024;15(1):2526. doi:10.1038/s41467-024-46829-0
34. Pham TCP, Dollet L, ea AMS. TNIK is a conserved regulator of glucose and lipid metabolism in obesity. *Sci Adv.* 2023;(9):32.
35. Deng Y, Liu X, Xie M, et al. Obesity enables NLRP3 activation and induces myocardial fibrosis via hyperacetylation of HADHA. *Diabetes.* 2023;72(11):1597–1608. doi:10.2337/db23-0264
36. Hogan MF, Hull RL. The islet endothelial cell: a novel contributor to beta cell secretory dysfunction in diabetes. *Diabetologia.* 2017;60(6):952–959. doi:10.1007/s00125-017-4272-9
37. Liu Z, Gan L, Xu Y, et al. Melatonin alleviates inflammasome-induced pyroptosis through inhibiting NF-kappaB/GSDMD signal in mice adipose tissue. *J Pineal Res.* 2017;63(1). doi:10.1111/jpi.12414.
38. Lebreton F, Berishvili E, Parnaud G, et al. NLRP3 inflammasome is expressed and regulated in human islets. *Cell Death Dis.* 2018;9(7):726. doi:10.1038/s41419-018-0764-x
39. Li G, Liu H, Ma C, Chen Y, Wang J, Yang Y. Exosomes are the novel players involved in the beneficial effects of exercise on type 2 diabetes. *J Cell Physiol.* 2019;234(9):14896–14905. doi:10.1002/jcp.28319
40. Pirozzi C, Coretti L, Opallo N, et al. Palmitoylethanolamide counteracts high-fat diet-induced gut dysfunction by reprogramming microbiota composition and affecting tryptophan metabolism. *Front Nutr.* 2023;10:1143004. doi:10.3389/fnut.2023.1143004
41. Verano-Braga T, Martins ALV, Motta-Santos D, Campagnole-Santos MJ, Santos RAS. ACE2 in the renin-angiotensin system. *Clin Sci (Lond).* 2020;134(23):3063–3078. doi:10.1042/CS20200478
42. Garg M, Royce SG, Tikellis C, et al. Imbalance of the renin-angiotensin system may contribute to inflammation and fibrosis in IBD: a novel therapeutic target? *Gut.* 2020;69(5):841–851. doi:10.1136/gutjnl-2019-318512
43. Jaworska K, Koper M, Ufnal M. Gut microbiota and renin-angiotensin system: a complex interplay at local and systemic levels. *Am J Physiol Gastrointest Liver Physiol.* 2021;321(4):G355–G366. doi:10.1152/ajpgi.00099.2021
44. Slonchak A, Clarke B, Mackenzie J, Amarilla AA, Setoh YX, Khromykh AA. West Nile virus infection and interferon alpha treatment alter the spectrum and the levels of coding and noncoding host RNAs secreted in extracellular vesicles. *BMC Genomics.* 2019;20(1):474. doi:10.1186/s12864-019-5835-6
45. Wu X, Gao Y, Xu L, et al. Exosomes from high glucose-treated glomerular endothelial cells trigger the epithelial-mesenchymal transition and dysfunction of podocytes. *Sci Rep.* 2017;7(1):9371. doi:10.1038/s41598-017-09907-6
46. Cecchin R, Troyer Z, Witwer K, Morris KV. Extracellular vesicles: the next generation in gene therapy delivery. *Mol Ther.* 2023;31(5):1225–1230. doi:10.1016/j.ymthe.2023.01.021
47. Gupta D, Zickler AM, El Andaloussi S. Dosing extracellular vesicles. *Adv Drug Deliv Rev.* 2021;178:113961. doi:10.1016/j.addr.2021.113961

International Journal of Nanomedicine

Dovepress

## Publish your work in this journal

The International Journal of Nanomedicine is an international, peer-reviewed journal focusing on the application of nanotechnology in diagnostics, therapeutics, and drug delivery systems throughout the biomedical field. This journal is indexed on PubMed Central, MedLine, CAS, SciSearch®, Current Contents®/Clinical Medicine, Journal Citation Reports/Science Edition, EMBASE, Scopus and the Elsevier Bibliographic databases. The manuscript management system is completely online and includes a very quick and fair peer-review system, which is all easy to use. Visit <http://www.dovepress.com/testimonials.php> to read real quotes from published authors.

Submit your manuscript here: <https://www.dovepress.com/international-journal-of-nanomedicine-journal>